Effect of the Anchoring Group on Electron Injection: Theoretical Study of Phosphonated Dyes for Dye-Sensitized Solar Cells

ARTICLE *in* THE JOURNAL OF PHYSICAL CHEMISTRY C · JANUARY 2012

Impact Factor: 4.77 · DOI: 10.1021/jp209823t

3 AUTHORS, INCLUDING:

Natalia Martsinovich
The University of Sheffield
60 PUBLICATIONS **865** CITATIONS

THE JOURNAL OF PHYSICAL CHEMISTRY C

ARTICLE

pubs.acs.org/JPCC

Effect of the Anchoring Group on Electron Injection: Theoretical Study of Phosphonated Dyes for Dye-Sensitized Solar Cells

Francesco Ambrosio, Natalia Martsinovich,* and Alessandro Troisi

Department of Chemistry and Centre for Scientific Computing, University of Warwick, Coventry, CV4 7AL, U.K.

ABSTRACT: The attachment chemistry of the chromophore onto the semiconductor surface influences the efficiency of electron injection in dye-sensitized solar cells (DSSCs). In this work, we study injection times for dyes that bind to the semiconductor surface via the phosphonic acid anchoring group and the effect on the injection time of different binding modes (molecular or dissociative, monodentate or bidentate) of phosphonic acid for both TiO_2 rutile (110) and anatase (101) surfaces. We calculate electron injection times for a large set of organic dyes on TiO_2 rutile (110) and anatase (101) surfaces for the most stable adsorption geometries of the phosphonic acid anchoring group, using a model based on partitioning the semiconductor−chromophore system into fragments. We analyze the influence of the size and nature of the anchoring group on the injection times, performing calculations with larger models of the anchoring group (e.g., phenyl-phosphonic acid). Through the partitioning procedure, we are able to separate the effect of the binding geometry from other effects influencing the efficiency of the electron injection. The results show that dissociative bidentate adsorption modes generally lead to faster injection, compared to monodentate and molecular ones, similar to the results obtained earlier for analogous carboxylated dyes. Our results are in good agreement with experiments (where available), showing that our model is capable of predicting the effects of the anchoring groups and of different spacer groups on the injection times and is therefore suitable for designing new and more efficient chromophores.

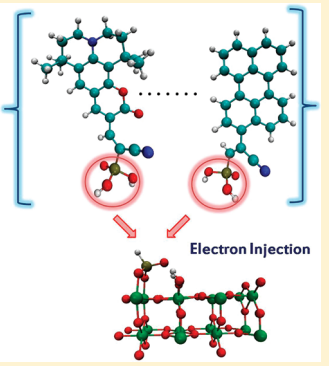

1. INTRODUCTION

Dye-sensitized solar cells (DSSCs) are one of the most promising technologies in the field of solar energy:[1−4] reaching the efficiency of solar light to electricity conversion up to 11%,[5,6] they represent one of the viable commercial alternatives to the common silicon-based cells. This kind of device is typically composed of a wide band gap semiconductor (TiO_2 or, less commonly, ZnO) deposited on a transparent conducting substrate, a molecular sensitizer (the dye) anchored on the semiconductor, and a redox electrolyte in solution and in contact with a counter electrode. In DSSCs, solar radiation is absorbed by the dye which, in its excited state, transfers an electron to the conduction band of the semiconductor. The dye is neutralized by the redox mediator in solution, which is regenerated by reduction at the counter electrode. This process generates a photovoltage between the semiconductor and the counter electrode. While the maximum efficiency is theoretically predicted around 30%,[7] the energy produced by this kind of cell is dramatically reduced by several loss mechanisms,[8] in particular, thermal de-excitation and charge recombination at the interface to the dye or to the electrolyte.[9,10] It is known from experimental measurements that the electron injection occurs on a time scale of femtoseconds to hundreds of femtoseconds[11−20] and is usually the fastest process.[15,21] Therefore, slower processes, such as the regeneration of the dye and of the redox couple and the electron transport through semiconductor nanoparticles, represent the efficiency determining steps of the device.[9] Nevertheless, fast electron injection, while not being a sufficient condition for a high-efficiency device, is surely a necessary requirement: slow electron injection is likely to lead to poor performance of the solar cell. In this framework, the study of the rates and mechanisms of electron injection and the design of efficient dyes is crucial.

The dynamics of photoinduced electron transfer processes at the dye−semiconductor interface has been studied with different approaches and methods in the past. Thoss and co-workers developed an ab initio based method, called the multilayer multiconfiguration time-dependent Hartree (ML-MCTDH) method.[22] In this variational approach, they employed a representation of Hamiltonian in a basis of localized donor and acceptor states, with the parameters of the Hamiltonian taken from ab initio calculations.[23−25] Prezhdo's group used nonadiabatic molecular dynamics to simulate electron transfer on time scales of up to tens of femtoseconds and to distinguish between adiabatic and nonadiabatic electron transfer pathways. For example, electron dynamics and electron transfer rates at the alizarine/TiO_2 interface were studied.[26−29] However, even if an ab initio description of the interface is appealing, this kind of time-resolved simulation is still rare and computationally demanding. Batista and co-workers used ab initio molecular dynamics (within density functional theory (DFT)) and adopted model Hamiltonian derived using the semiempirical extended

Received: October 12, 2011
Revised: December 14, 2011
Published: December 21, 2011

Hückel approach to describe the excited states and propagate the wave function in time, for representative nuclear configurations. In this way, they modeled the dye−semiconductor electron transfer and subsequent charge delocalization in TiO_2 crystals.[30,31] May and co-workers studied the heterogeneous electron transfer for the TiO_2−perylene derivatives system using a diabatic-like separation of the whole system into molecular and semiconductor states and considered the ground and first excited state for the dye together with a large number of states in the conduction band of the semiconductor.[16,32] This model is based on experimental results since the Hamiltonian features parameters that are fitted to measured spectra. Most of these models require a simulation of a complete semiconductor−chromophore system and are therefore not suitable for the screening of properties of large numbers of chromophores.

Our group developed a computational approach based on partitioning the TiO_2−dye system into three subsystems: surface, surface−dye interface, and isolated dye components.[33] It has been shown that the electron injection rate can be obtained from a set of parameters that are accessible from computational chemistry methods: (i) the coupling between the semiconductor's and dye's atomic orbitals, (ii) the semiconductor's energy-dependent density matrix, and (iii) the dye's lowest unoccupied molecular orbital (LUMO) coefficients; (ii) and (iii) depend only on the semiconductor and on the dye, respectively, and (i) is approximately the same for all dyes which share the same adsorption mode on the surface. For each dye with the same attachment chemistry to TiO_2, it is therefore possible to evaluate the rate only by computing its LUMO coefficients and energy and using the density matrix and coupling calculated for the generalized interface (a generalization to cases where the lowest excited state is not dominated by the dye's HOMO→LUMO transition is simple). This model is suitable for fast evaluation of injection times, as it does not require a time-consuming simulation of a complete semiconductor−chromophore system and does not rely on experimental data. It was applied to study injection times in a series of organic dyes, including perylene derivatives, isonicotinic and biisonicotinic acid, and coumarin.[33,34] The obtained results were in good agreement with the available experimental injection times and were compatible with the power conversion efficiencies of DSSCs based on these dyes.

In this work, we employ the same method, to study the injection characteristics of dyes that bind to the semiconductor surface with a phosphonate moiety and to analyze the effects of the attachment chemistry on injection rates. These kinds of dyes are very interesting for DSSC devices; in fact, theoretical studies of phosphonic acid show that it binds more strongly than formic acid to TiO_2 surfaces.[35,36] Therefore, the use of phosphonated dyes can improve the long-term stability of the DSSC device. However, there are few experimental and theoretical studies of the electron injection characteristics of phosphonated dyes. Experimental studies of perylene derivatives on TiO_2 suggest that electron injection from phosphonated dyes is somewhat slower than from their carboxylated analogues.[17−20,37,38] This result is supported by theoretical studies of the same molecules, using the full width at half-maximum (fwhm) of the dye's LUMO state as a measure of injection time[25] and using model Hamiltonian calculations.[25,35] However, there is no definite agreement between the theoretical predictions made using different computational approaches. For example, for pyridine-4-phosphonic acid, calculated injection times range from 10 fs (using parametrized Hamiltonian[25]) to 460 fs (using a semiempirical Hückel Hamiltonian combined with molecular dynamics[39]). Moreover, theoretical modeling suggests that injection times strongly depend on the adsorption mode (e.g., 60 fs injection time for the bidentate mode and 460 fs for the monodentate adsorption of the above molecule).[39] Therefore, at present, there is no systematic study of phosphonated dyes, and among these few studies, there is a significant discrepancy between different methods and with experimental results too. Moreover, the attachment chemistry of phosphonic acid on TiO_2 and the effects of the different binding modes on the injection characteristics have not been considered yet. This is an important aspect because the theoretical descriptions of the electronic structure at the interface and, consequently, of the charge transfer need an accurate description of the adsorption geometry of the dye.

Several theoretical studies addressed the adsorption geometry of phosphonic or methylphosphonic acid on rutile (110) and anatase (101), using DFT[35,36,41] and density functional tight-binding (DFTB).[40] A large number of possible configurations have been identified: four on rutile (110) and eight on anatase (101). Thus, phosphonic acid has a much richer adsorption chemistry on TiO_2 than seen for carboxylic acids, which have one stable adsorption configuration on rutile (110) (dissociated bidentate)[42,44,45] and two configurations on anatase (101) (molecular monodentate adsorption and dissociative bridging-bidentate).[43,45] For phosphonic acid, the bidentate configurations were identified as the most stable ones on rutile (110), particularly the fully dissociative one with two protons adsorbed on the semiconductor surface.[35,40] On anatase (101) slabs, DFT B3LYP calculations favored the monodentate configuration,[36] while DFTB studies favored the bidentate configuration with two protons adsorbed on the surface,[40] even if the differences between the best monodentate and bidentate structures in both of these studies were no more than 0.2 eV (of the order of the accuracy of DFT calculations and smaller than the accuracy of DFTB calculations). These results suggest that different adsorption modes are likely to coexist, and an accurate theoretical prediction of the injection times of phosphonated dyes must take into account and analyze the effects of the different adsorption modes.

The present work is organized as follows. A brief outline of our theoretical model and the details of the computational procedure are given in Section 2. In Section 3, we present our calculated electron injection times for a large set of phosphonated organic dyes for the most stable adsorption modes on TiO_2 rutile (110) and anatase (101) surfaces. We compare the calculated injection times with experimental values (where available), showing satisfactory agreement between our theoretical values and the experiments. We analyze the effects of the different binding modes on the injection time, identifying the configurations leading to faster injection, for both rutile (110) and anatase (101). We study the effect of the size and of the chemical match of the anchor group. Finally, we compare our results for the considered set of dyes with the ones previously obtained for their carboxylated analogues.

2. METHOD AND COMPUTATIONAL DETAILS

2.1. Model of Electron Transfer. We compute the injection times, adopting the method developed and used in recent publications by our group.[33,34] We define charge injection as a charge transfer process between an orbital localized on the chromophore molecule ($|s\rangle$) and one of the one-electron states of the continuum formed by the semiconductor's conduction

band states (the family of states $\{|l\rangle\}$). The orbital localized on the chromophore can be identified with its LUMO if the excited state is dominated by the HOMO→LUMO transition (as shown to be the case for many organic chromophores,[46,47] including, for example, coumarin-based chromophores studied in this work[48]). $|s\rangle$ and $|l\rangle$ can be expressed in terms of localized basis functions, i.e., a linear combination of atomic orbitals: $|s\rangle = \sum_m c_m \chi_m$ and $|l\rangle = \sum_k C_{kl}\phi_k$ where $\{\chi_m\}$ is the basis set for the molecule and $\{\phi_k\}$ is the basis set for the semiconductor. The indices m (or n) and k (or k') refer to the molecule's and the semiconductor's basis functions, respectively. We can define the semiconductor's energy-dependent density matrix as $\rho_{kk'}(E) = \sum_l C_{lk} C^*_{lk'} \delta(E - E_l)$, where E_l are the energies of the one-electron states on the semiconductor. We further define the matrix elements V_{mk} as the electronic coupling between localized atomic orbitals on the semiconductor and on the dye. Following these definitions, we have shown in ref 33 that the rate of electron injection Γ (for orthogonal basis sets, such as those used in our current calculations) can be expressed as

$$\hbar\Gamma = 2\pi \sum_{m,n} c_m c_n^* \sum_{k,k'} V_{mk} V^*_{nk'} \rho_{kk'}(E_s) \quad (1)$$

For nonorthogonal basis sets, the above equation is modified as follows[33]

$$\hbar\Gamma = 2\pi \sum_{m,n} c_m c_n^* \sum_{k,k'} (ES_{mk} - V_{mk})(ES_{nk'} - V_{nk'})^* \rho_{kk'}(E_s) \quad (2)$$

where S_{mk} and $S_{nk'}$ are the overlap matrix elements.

To calculate the injection time, one needs (i) a computation of the local density of states of the semiconductor $\rho_{kk'}(E)$, (ii) a computation of the coupling $\{V_{mk}\}$ between the semiconductor's and molecule's localized basis functions, and (iii) a computation of the molecular orbital coefficients $\{c_m\}$ and the energy of the molecule's LUMO, which is the injection energy E_s in eqs 1 and 2.

Because of the localized nature of atomic orbitals, the coupling terms V_{mk} between the semiconductor's and molecule's localized basis functions are significantly different from zero only for those m, k that are at or near the semiconductor−dye interface. Hence, we can use the $\rho_{kk'}(E)$ matrix elements only for k, k' close to the semiconductor surface. In our model, therefore, we represent a semiconductor surface with a slab, which is periodically repeated in two dimensions and has a finite depth, a widely used approach for modeling surfaces. Then, to obtain V_{mk} values, instead of performing a calculation of an entire adsorbed dye, which is very computationally demanding and would not be feasible in screening a large number of potential chromophores, we can consider only the interface of the semiconductor slab with the chromophore's anchoring group. In fact, since we expect V_{mk} values to be large only in the interface region, V_{mk} values for m not belonging to the anchoring group are going to be negligible and can be considered to be zero. Of course, the difference between the V_{mk} matrix elements for different attachment chemistries is ultimately responsible for the different injection times.

2.2. Electronic Structure Calculations. To obtain V_{mk}, C_{lk}, and c_m terms, we modeled the TiO_2 + anchoring group system, as well as the isolated dye molecules, using DFT calculations. We used the CRYSTAL09 code.[49] CRYSTAL09 computations employed an explicit all-electron representation of TiO_2 with triple valence plus polarization Gaussian basis sets first used in ref 50 for Ti and O and a double valence plus polarization Gaussian basis set first used in ref 51 for P (these basis sets are available on the CRYSTAL Web site[52]). We employed the B3LYP functional[53] which was proven to give a reasonable description of the TiO_2 electronic structure.[54] The **k**-points sampled were chosen using a Monkhorst−Pack net using a $2 \times 2 \times 1$ **k**-point grid for slabs with adsorbates. The convergence criteria used for geometry optimization were: energy tolerance 10^{-4} Ha, root-mean-square (rms) of the gradient 10^{-3} Ha/Bohr, rms of the displacement 0.0012 Bohr. Rutile (110) and anatase (101) surfaces were both modeled using two-layer slabs with the 2×2 cell area (Figure 1a,b). The modeling of molecular adsorption was obtained using constrained slabs with the adsorbate placed at one side of the slab and the bottom layer atoms fixed at their respective bulk geometry. This scheme is used in the majority of simulations of surfaces, including TiO_2.[43−45,54]

A similar computational setup (CRYSTAL calculations using B3LYP functional and the same convergence criteria as above) was used to model isolated dye molecules, but in this case the simulated system was nonperiodic. Double valence plus polarization Gaussian basis sets, available on the CRYSTAL Web site,[52] were used for C, N, and P, and a triple valence plus polarization Gaussian basis set was used for O.

2.3. Surface−Adsorbate Systems. In the majority of the calculations discussed below (unless noted otherwise), phosphonic acid on TiO_2 was used to represent the TiO_2−anchoring group interface. There are several alternative adsorption modes for such anchoring groups as carboxylic and phosphonic acid, e.g., molecular, bridging, or chelating. A large number of adsorption modes were reported for phosphonic (and alkylphosphonic) acids on TiO_2: up to four on rutile (110)[35,40,41] and eight on anatase (101),[36,40] including both bidentate and monodentate, with and without the acidic proton transferred to the surface. As a starting point for modeling the different adsorption modes of phosphonic acid (and phosphonic acid functionalized with organic groups), we choose the structures studied in the work of Luschtinetz and co-workers, who computed four adsorption geometries for rutile (110) and eight for anatase (101).[40] For consistency, and to verify that the predicted structures are not modified by a different computational method, we reoptimize Luschtinetz's structures.

In Figure 1a and Figure 1b, we show the optimized structures for the adsorption of phosphonic acid on the rutile (110) and the anatase (101) surfaces. For rutile, the m1 and m2 structures feature a monodentate adsorption mode, molecular and dissociative with a proton transferred to a surface O, respectively. The latter, according to previous theoretical work,[40] is more stable than the former by ≈9 kcal/mol. The b1 and b2 structures show a bidentate adsorption mode with one and two adsorbed protons, respectively, and they are the most stable adsorption modes, a result which is confirmed by a recent study of adsorption of methyl phosphonate on rutile (110).[41] The b2 structure is the most stable adsorption configuration, due to the adsorption of both protons on the slab surface (≈5 kcal/mol more than the b1 structure). Our results agree with this picture of the system, with the m2 mode being the most stable monodentate (≈10 kcal/mol more than m1) and with the b2 mode being the most stable adsorption mode (≈20 kcal/mol more than the b1 structure) overall.

For anatase (101), although previous studies considered eight adsorption configurations,[36,40] we choose to study only the four most stable ones. We have a monodentate molecular adsorption mode (m1) and three bidentate modes, two of them with a single

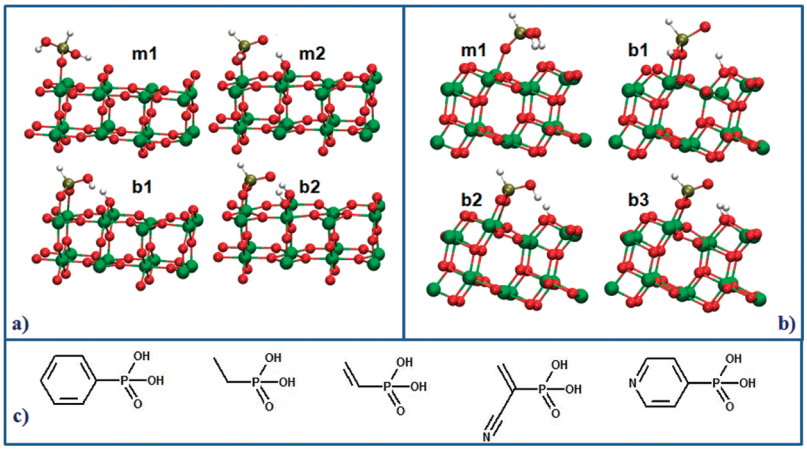

Figure 1. Optimized structures (a) of the two-layer rutile (110) slab with phosphonic acid and (b) of the two-layer anatase (101) slab with phosphonic acid systems with different adsorption modes. Ti atoms are in green, O in red, P in brown, and H in white (see text for the description of the adsorption modes). (c) Structures of the studied larger binding groups.

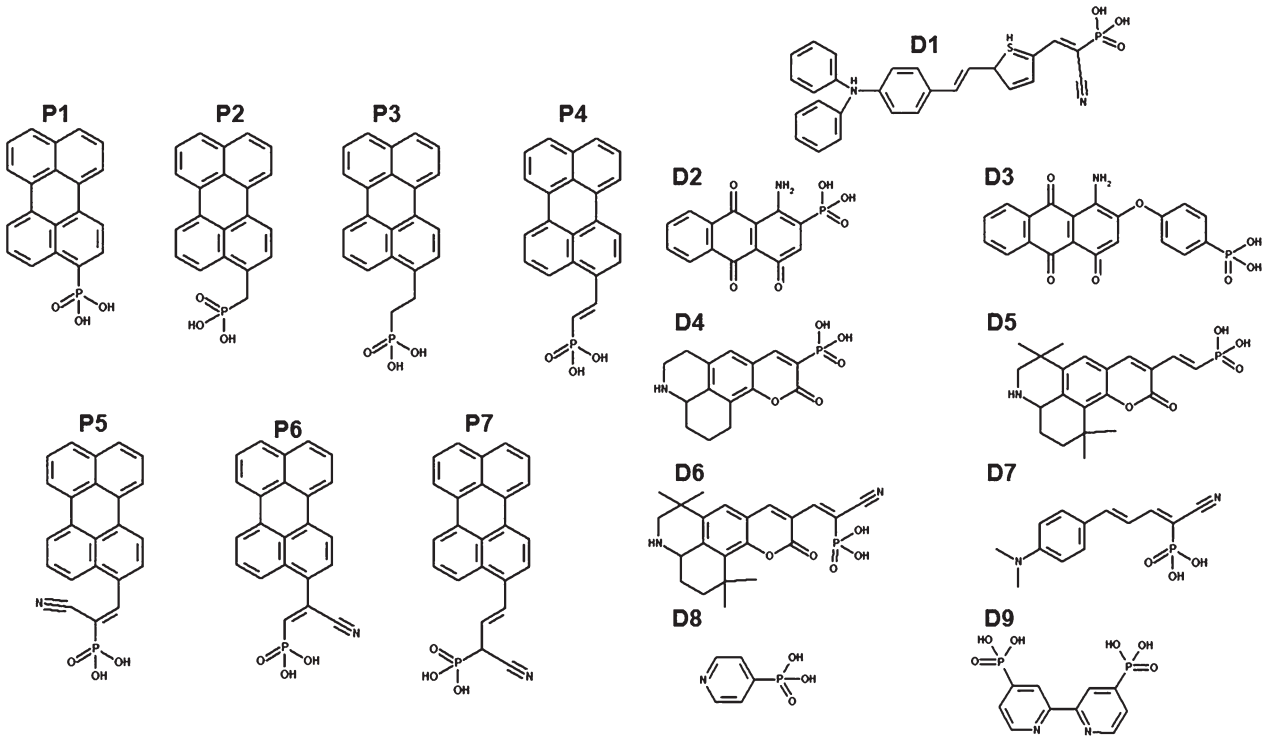

Figure 2. Structures of the studied perylene derivatives (P1−P7) and of the other chromophores (D1−D9).

proton adsorbed on the surface (b1 and b2) and one with both protons adsorbed on the slab (b3). Luschtinetz and co-workers, using DFTB, found that bidentate modes, in particular the b3 adsorption mode, represent the most stable binding geometry (the difference with the least stable considered bidentate mode is ≈5 kcal/mol, while the difference with the most stable monodentate mode is around ≈20 kcal/mol),[40] while an earlier work by Nilsing and co-workers,[36] using DFT-B3LYP, suggests that the m1 structure has the strongest adsorption (relative adsorption energies are contained in a small range, ≈7 kcal/mol, for all the studied configurations). Nevertheless, these earlier studies agree that the difference in stability of the various adsorption modes is small. In our study, the most stable adsorption mode is the b3; the difference between b3 and the least stable considered bidentate (b1) is 12 kcal/mol, and the difference with the most stable monodentate is 16 kcal/mol. Our structures are in good agreement with previous works, and the P−H bond in all these configurations is pointing upward, compatible with possible adsorption geometries of a complete chromophore on the slab.

Additionally, we performed several calculations using larger anchoring group models: instead of just the phosphonic acid group, we considered larger fragments of the dyes (i.e., phosphonic acid with various spacer groups, shown in Figure 1c), adsorbed on the rutile (110) surface. For these substituted

dx.doi.org/10.1021/jp209823t |J. Phys. Chem. C 2012, 116, 2622–2629

Table 1. Calculated and Experimental (Where Available) Injection Times (fs) of the P1−P7 Dyes on Rutile (110) for Their m1, m2, b1, and b2 Adsorption Modes and on Anatase (101) for their m1, b1, b2, and b3 Adsorption Modes, Respectively

dye on rutile	t_{m1} (fs)	t_{m2} (fs)	t_{b1} (fs)	t_{b2} (fs)	t_{exp} (fs)[38]
P1	14.8	7.6	2.6	2.9	23.5
P2	150.3	117.9	40.2	73.2	35.9
P3	42.8	67.9	28.0	33.4	
P4	27.8	33.1	8.3	4.9	
P5	22.6	10.2	2.8	3.3	
P6	3.4	2.8	1.55	1.5	
P7	136.2	213.9	44.0	14.2	
dye on anatase	t_{m1} (fs)	t_{b1} (fs)	t_{b2} (fs)	t_{b3} (fs)	t_{exp} (fs)[37]
P1	2.9	1.6	2.4	0.44	28
P2	176.0	123.4	41.5	9.6	63
P3	177.8	18.0	27.3	2.1	
P4	35.8	1.5	4.5	0.32	
P5	63.4	6.1	1.7	0.87	
P6	2.3	2.9	0.4	0.13	
P7	15.1	90.0	9.5	19.4	

phosphonic acids, we used the same adsorption modes (m1, m2, b1, and b2) as for the phosphonic acid on rutile (110). These calculations were done to check if the size of the anchoring fragment used in the TiO_2-anchoring group interface model affects the accuracy of the calculated injection times.

3. RESULTS AND DISCUSSION

We chose a set of dye molecules featuring phosphonic acid as a binding group (Figure 2). Among them, there are some perylene derivatives whose charge injection on rutile and anatase surfaces has been studied experimentally (P1−P2),[37,38] but we also model some new perylene derivatives (P3−P7) to explore the effect of simple modification of the spacer group chemistry near the phosphonic acid anchoring group. We have also considered a set of dyes (D1−D9 in Figure 2), similar to those studied in an earlier work,[34] but with the carboxylic group replaced by the phosphonic group, to evaluate the difference between these two anchoring groups. In Table 1 we collect the injection times for the P1−P7 dyes on rutile (110) and anatase (101), respectively. First, we compare the obtained results with the known experimental values for the P1 and P2 dyes on rutile (110) and on anatase (101). For the P1 dye on rutile (110), we compute the injection times of 2.6 and 2.9 fs for the most stable adsorption modes (b1 and b2), somewhat faster than the experimental value of 23.5 fs, while for P2 we obtain 40.2 and 73.2 fs, similar to the experimental result (35.9 fs). Injection times for the less stable adsorption modes m1 and m2 are slower than for b1 and b2. For the P1 dye on anatase (101), the computed injection times are smaller than the experimental value (28 fs) for all the adsorption modes (between 0.44 and 2.9 fs), while for P2 dye the computed injection times are also somewhat smaller for the bidentate adsorption modes but slightly larger than the experimental time for the monodentate adsorption modes. The agreement between the calculated and experimental values is reasonably good (within an order of magnitude—which is acceptable considering

Table 2. Comparison of the Injection Times (fs) for P3, D6, and D8 Dyes on Rutile (110), Calculated with Different Models of the Anchoring Group

dye	anchor group	t_{m1} (fs)	t_{m2} (fs)	t_{b1} (fs)	t_{b2} (fs)
P3	$HPO(OH)_2$	42.8	67.9	28.0	33.4
	$CH_3-CH_2-PO(OH)_2$	24.5	64.2	34.3	21.0
D6	$HPO(OH)_2$	6.3	3.2	1.8	2.3
	$CH_2=CH-PO(OH)_2$	5.5	3.5	2.3	1.3
	$CH_2=C(CN)-PO(OH)_2$	6.5	2.3	1.8	1.6
D8	$HPO(OH)_2$	7.3	1.5	0.54	0.76
	$Ph-PO(OH)_2$	1.03	0.92	1.3	0.73
	$Py-PO(OH)_2$	3.6	0.93	1.1	0.46

that experimental estimates of injection times are often the upper limits of injection times, limited by the instrument resolution, which ranges from a few femtoseconds[20] to as high as 100 fs,[11−14] depending on the technique used).

We observe that injection is faster for the most stable adsorption modes (the bidentate ones) and that there is no remarkable difference between the injection times calculated for rutile (110) and anatase (101). Nevertheless, we can pinpoint that the anatase b3 adsorption mode features the fastest injection for all the dyes. We observe that the effect of the different attachment modes on the injection time is more evident for slower dyes, while for the fast dye P1 the difference between the adsorption modes is less pronounced. Unfortunately, there is experimental data only for few perylene−phosphonic dyes, but this theoretical study of their charge injection properties is useful because it allows us to analyze systematically the efficiency of different dyes, e.g., with different spacer groups. For example, we observe similar results for the P2 and P3 dyes (which feature a CH_2 and a CH_2CH_2 spacer group, respectively) with slower injection than the simple P1 dye, due to the presence of the sp^3 carbon atoms separating the aromatic part of the dyes from the anchoring group. On the other hand, the injection is remarkably fast for the P4 dye, which contains the CH=CH spacer group, an effect that has already been observed for carboxylic acid-binding dyes.[34,37]

In the P5 and P6 dyes, we study the effect of the CN moiety on the injection times, placing this group in two different positions. In P5, we place it on the same sp^2 carbon linked to the $PO(OH)_2$ moiety (a motif used in many carboxyl-containing dyes).[55] In the P6 dye, we investigate an alternative position of the cyano group on the next sp^2 carbon atom, in the β position to the phosphonate group, which has not been considered so far for DSSC dyes, to the best of our knowledge. The results for the two chromophores are similar, featuring a very fast injection due to the presence of the CN moiety, which is a strong electron-withdrawing group. This agrees with experiments reporting that dyes with the CH=CH connected to the cyano group lead to an increased efficiency in the DSSC device.[55] It is worth noting that injection from the P6 dye (with the new position of the cyano group) is slightly faster than P5, suggesting that this novel attachment chemistry may be used to realize more efficient charge injection in DSSC dyes.

Finally, we study the P7 dye that we conceived to analyze the effect of the different groups at the same time: it contains the vinyl group, an sp^3 carbon, and a CN moiety attached to it. The results show an injection which is faster than for P2 and P3 dyes but slightly slower than for the other dyes, as we could expect knowing the effect of the different groups: the CN group in P7 ensures faster

Table 3. Injection Times (fs) of the P1−P7 and D1−D9 Dyes on Rutile (110) for the m1, m2, b1, and b2 Adsorption Geometries, Respectively, and Injection Times of the Same Dyes Featuring Carboxylic Acid as a Binding Group Calculated in This Work and from the Literature[34]

dye	t_{m1} (fs)	t_{m2} (fs)	t_{b1} (fs)	t_{b2} (fs)	t_{COOH} (fs)	t_{COOH} (fs) ref 34	t_{b2}/t_{COOH} ratio[a]
P1	14.8	7.6	2.6	2.9	6.5	5.3	0.44
P2	150.3	117.9	40.2	73.2	269.5		0.27
P3	42.8	67.9	28.0	33.4	109.9	282.0	0.30
P4	27.8	33.1	8.3	4.9	11.7	6.0	0.42
P5	22.6	10.2	2.8	3.3	10.8		0.31
P6	3.4	2.8	1.55	1.5	3.4		0.44
P7	136.2	213.9	44.0	14.2	30.7		0.46
D1	19.8	5.1	3.1	3.9		17.2	0.23
D2	4.1	1.8	9.00	6.9		33.0	0.21
D3	210.2	126.0	81.9	71.8		157.0	0.46
D4	30.2	11.3	5.4	13.1		10.0	1.31
D5	14.5	13.7	12.4	29.8		11.6	2.57
D6	6.3	3.2	1.8	2.3		4.8	0.48
D7	5.1	4.0	2.9	1.4		5.6	0.25
D8	7.3	1.5	0.54	0.76		0.73	1.0
D9	4.5	3.2	0.51	1.0		0.68	1.47

[a] Ratios between injection times for carboxylated and phophonated dyes (for the former we consider our values for the P1−P7 dyes and ref 34 values for D1−D9 dyes; for the latter, we consider the injection times belonging to the most stable adsorption mode b2).

injection than for P2 and P3, but the presence of the sp^3 carbon slows injection compared to the dyes P1 and P4−P6 with all unsaturated carbons. These results suggest that, to some extent, the effect of these structural modifications is additive.

To validate one of the approximations used in this work, we investigate how the calculated injection time is affected by the size of the anchoring fragment in the TiO_2-anchoring group interface model, by including various spacer groups in the anchoring group (see Figure 1a and Table 2). For example, for the P3 dye we calculate injection times, employing phosphonate or ethyl-phosphonate adsorbed on TiO_2 as models for the TiO_2-anchoring group interface and obtain results in very good agreement with each other. For the D6 dye, we consider two alternative models of the interface, with anchoring groups containing the CH_2═CH and the CH_2═C(CN) moiety. The effect of the introduction of the double bond and of the cyano group in the anchoring group model does not affect the result significantly. Finally, we study the injection of D8, considering phenyl (Ph)-phosphonate and pyridyl (Py)-phosphonate as anchoring groups present in the interface model (in this case the latter represents also the complete dye), and the results are definitely very similar, in particular for the two different aromatic groups. This proves that the coupling terms between the dye's and semiconductor's orbitals are significant only immediately at the binding interface, and even a small model anchoring group, such as phosphonic acid, is sufficient to describe the interface, making the full dye-surface calculation not necessary in most cases.

In Table 3, we show the injection times calculated for the P1−P7 dyes and D1−D9 dyes on rutile (110) and compare them with the results for their carboxylated analogues. Injection times for similar dyes containing a carboxylic acid instead of a phosphonic acid group were recently studied by our group[34] (molecular monodentate and dissociative bidentate adsorption modes for anatase (101), dissociative bidentate for rutile (110); DFT-PBE level of theory). Here we compare injection times for carboxylic and phosphonic groups. First, we compare the earlier results for carboxylic-containing molecules (adsorbed on rutile (110) in the bridging-bidentate configuration),[34] computed using the PBE functional[56] within the SIESTA code,[57] with our new results computed using CRYSTAL09 and the B3LYP functional. Table 3 (columns 6 and 7 for P1−P7 dyes) clearly shows that the results obtained in this work are consistent with the PBE calculations, where the largest discrepancy arises for the P3 dye, and are in slightly better agreement with experimental values (which are 9 fs for P1, 47 fs for P3, and 13.5 fs for P4[38]). This shows that the choice of the exchange-correlation functional (pure DFT, e.g., PBE, or hybrid, e.g., B3LYP) does not strongly influence the alignment of the dyes' and semiconductor's electronic energy levels and the resulting electron injection times.

We can also compare the injection times calculated for dyes featuring the two different binding groups. While we can clearly state that the b2 mode for phosphonated dyes gives a faster injection (approximately twice as fast), compared to the carboxylated analogues for most of the considered dyes, the results for the two anchoring groups are similar, and the general trend is comparable.

Our ratio of carboxylated and phosphonated dyes' injection times is in disagreement with recent experimental[16,18,37,38] and theoretical reports,[15,25,35] where injection from carboxylated dyes was slightly faster. To reconcile this difference, we investigated the reasons why injection from phosphonated dyes in our calculations was faster than from carboxylated dyes. One possible reason is a difference in the LUMO energies of the carboxylated and phosphonated dyes. For dyes P1−P7, the differences in the calculated LUMO energies between carboxylated and phosphonated analogues ranged from almost zero (0.01 eV) for P2 and P3 to −0.29 eV for P5 (with the carboxylated dyes' LUMOs being generally lower, i.e., closer to the TiO_2 conduction band). Injection times for dyes P1−P7 (using the b2 adsorption mode on rutile (110)) were recalculated using their carboxylated analogues' LUMO energies; these new injection times were larger on average by 17%, and the change in injection time did not correlate with the change in the LUMO energy. Thus, the LUMO energies alone cannot account for the factor-of-two difference in the injection times of carboxylated and phosphonated dyes.

The other possible reason is the difference in the coupling coefficients for these two anchoring groups. We found, for the P1 dye as a model system, that in the case of the carboxylated dye the anchoring group's basis orbitals with the largest weight of the LUMO ($C_{COOH}(2p) > O_{COOH}(2p)$) have relatively low coupling with TiO_2 basis orbitals, while in the analogous phosphonated dye, the anchoring group's orbitals carrying a large proportion of the LUMO ($P_{PO3H2}(3p) \approx O_{PO3H2}(2p)$) have also a large coupling with TiO_2. Thus, the balance between the orbitals' coupling and the weight of the dyes' LUMO on the anchoring group is crucial, and it cannot be predicted intuitively and has to be computed.

We note that the theoretical works,[25,35] which obtained relatively slower injection from phosphonated dyes, used monodentate adsorption configurations, which, in our calculations, also give slower injection times than bidentate configurations and are slower or similar to injection from carboxylated dyes.

We point out that since the difference in stability of the different adsorption modes of phosphonic acid is small,[35,36,40] in the real system several adsorption modes are likely to coexist, and

the average injection times for phosphonated dyes are likely to be longer than the results for the b2 mode (by no more than an order of magnitude, according to the data in Table 3) and closer to an average value between the several most stable configurations.

In summary, we show that our model gives reliable estimates of injection times and can be used to predict injection properties of new dyes. Our results suggest that the phosphonic acid anchoring group is as good as the carboxylic acid group in DSSC dyes because its adsorption is stronger, while injection times are similar.

4. CONCLUSIONS

The objective of this work was to perform a systematic analysis of the electron injection characteristics and to explore the effect of the anchoring group for a large set of phosphonated dyes on TiO_2. To fulfill this goal, we adopt the partitioning scheme for the TiO_2−dye system, which allows us to compute the charge injection time, $1/\Gamma$, using the electronic properties of the fragments: density of states of TiO_2, TiO_2-anchoring group coupling, and dyes' LUMO wave function coefficients. In this way, we are able to quickly screen a large set of dyes: for each dye we need only a calculation of the isolated dye's electronic structure and the LUMO orbital since the TiO_2-anchoring group coupling is common for all the chromophores sharing the same attachment chemistry. We model the TiO_2-anchoring group system adopting phosphonic acid as the anchoring group, and we study the most stable adsorption modes on both rutile (110) and anatase (101) surfaces. We then compute the injection times for a large set of phosphonated dyes, for all considered adsorption modes.

Our study of the injection times for different binding geometries shows that dissociative bidentate adsorption modes generally lead to faster injection, compared to monodentate and/or molecular ones, for both rutile (110) and anatase (101). In particular, fully dissociative bidentate geometries with both hydroxyl protons of the $HPO(OH)_2$ moiety adsorbed on the semiconductor surface (which are the most stable adsorption configurations) provide the fastest injection. When we compare the injection times computed for phosphonated dyes on rutile (110) with the ones calculated for their carboxylated analogues, we find that the fastest adsorption modes (bidentate ones) on phosphonated dyes give faster injection times than in carboxylated dyes, while the monodentate modes are slower than the related carboxylated dyes. However, the difference in stability of the different adsorption modes of phosphonic acid on TiO_2 is small, and therefore, several modes are likely to coexist with the overall injection time being average between the times characteristic for the different adsorption modes.

From a methodological point of view, we show that the choice of exchange-correlation functional (PBE, a pure DFT functional based on the generalized gradient approximation (GGA), or the hybrid B3LYP functional) has no dramatic effect on the alignment of the dyes' and semiconductor's electronic energy levels and, therefore, on the calculated electron injection times. Our study of the size of the anchoring group shows that a very simple model, featuring only the phosphonic acid attached to the surface, is sufficient to simulate the TiO_2−dye interface. Finally, we point out that the partitioning scheme allows us to isolate the effect of the anchoring group from other effects that we have not included (e.g., solvent effect and possible mismatch of energy levels). Therefore, this method gives an opportunity to identify design rules for DSSC dyes. By comparison, a global approach that would include all the chemical components and all these effects in a single calculation may be more accurate for the study of a single particular case but is not capable of providing specific insights into the influence of different effects.

We demonstrate that our predictions are in good agreement with the available experimental results and that our model is capable of predicting the effects of different spacer groups on the injection times, thus being suitable for designing new and more efficient chromophores. In this way, we can assist experimental studies, providing a reliable qualitative and quantitative prediction of the injection characteristics of a dye before it has been synthesized. As an example, we analyze the effect of the chemical characteristics of different groups, in particular the effect of the electron-withdrawing group CN. We verify its effect on injection times by placing it in different positions, and we propose a new slightly modified anchoring group that gives very fast injection (structure P6, with the CN group attached to the sp^2 carbon in the beta position to the $PO(OH)_2$ moiety). Natural extension of our method includes calculations of injection times for other less common binding groups (e.g., sulfonated dyes) and the extension of the study to metal−organic dyes and to different semiconductors (i.e., ZnO).

AUTHOR INFORMATION

Corresponding Author

*E-mail: n.martsinovich@warwick.ac.uk.

ACKNOWLEDGMENT

We acknowledge financial support from the European Research Council (ERC) and Engineering and Physical Sciences Research Council (EPSRC).

REFERENCES

(1) O'Regan, B.; Grätzel, M. *Nature* **1991**, *353*, 737–740.
(2) Grätzel, M. *J. Photochem. Photobiol. C* **2003**, *4*, 145–153.
(3) Moreira Gonçalves, L.; de Zea Bermudez, V.; Aguilar Ribeiro, H.; Magalhães Mendes, A. *Energy Environ. Sci.* **2008**, *1*, 655–667.
(4) Preat, J.; Jacquemin, D.; Perpète, E. A. *Energy Environ. Sci.* **2010**, *3*, 891–904.
(5) Chiba, Y.; Islam, A.; Watanabe, Y.; Komiya, R.; Koide, N.; Han, L. Y. *Jpn. J. Appl. Phys.* **2006**, *45*, L638–L640.
(6) Kroon, J. M.; Bakker, N. J; Smit, H. J. P.; Liska, P.; Thampi, K. R.; Wang, P.; Zakeeruddin, S. M.; Grätzel, M.; Hinsch, A.; Hore, S.; et al. *Prog. Photovoltaics Res. Appl.* **2007**, *15*, 1–18.
(7) Hagfeldt, A.; Boschloo, G.; Sun, L.; Kloo, L.; Pettersson, H. *Chem. Rev.* **2010**, *110*, 6595–6663.
(8) O' Regan, B. C.; Durrant, J. R. *Acc. Chem. Res.* **2009**, *42*, 1799–1808.
(9) Durrant, J. R.; Haque, S. A.; Palomares, E. *Coord. Chem. Rev.* **2004**, *248*, 1247–1257.
(10) Prezhdo, O. V.; Duncan, W. R.; Prezhdo, V. V. *Acc. Chem. Res.* **2008**, *41*, 339–348.
(11) Murakoshi, K.; Yanagida, S.; Capel, M.; Castner, E. W. *Nanostructured Materials*; American Chemical Society: Washington DC, 1997; Vol. 679, Chapter 17, pp 221−238
(12) Wachveitl, J.; Huber, R.; Spörlein, S.; Moser, J. E.; Grätzel, M. *Int. J. Photoenergy* **1999**, *1*, 1–3.
(13) Huber, R.; Moser, J. E.; Grätzel, M.; Wachveitl, J. *Chem. Phys.* **2002**, *285*, 39–45.
(14) Hao, E. C.; Anderson, N. A.; Asbury, J. B.; Lian, T. Q. *J. Phys. Chem. B* **2002**, *106*, 10191–10198.
(15) Frontiera, R. R.; Dasgupta, J.; Mathies, R. A. *J. Am. Chem. Soc.* **2009**, *131*, 15630–15633.
(16) Wang, L.; Ernstorfer, R.; Willig, F.; May, V. *J. Phys. Chem. B* **2005**, *109*, 9589–9595.

(17) Ernstorfer, R.; Gundlach, L.; Felber, S.; Storck, W.; Eichberger, R.; Willig, F. *J. Phys. Chem. B* **2006**, *110*, 25383–25391.
(18) Gundlach, L.; Ernstorfer, R.; Willig, F. *J. Phys. Chem. C* **2007**, *111*, 13587–13594.
(19) Gundlach, L.; Ernstorfer, F.; Willig, F. *Prog. Surf. Sci.* **2007**, *82*, 355–377.
(20) Gundlach, L.; Letzig, T.; Willig, F. *J. Chem. Sci.* **2009**, *121*, 561–574.
(21) Ghosh, H. N. *J. Phys. Chem. B* **1999**, *103*, 10382–10387.
(22) Wang, H. B.; Thoss, M. *J. Chem. Phys.* **2003**, *119*, 1289–1299.
(23) Kondov, I.; Thoss, M.; Wang, H. *J. Phys. Chem. A* **2006**, *110*, 1364–1374.
(24) Kondov, I.; Čižek, M.; Benesch, C.; Wang, H.; Thoss, M. *J. Phys. Chem. C* **2007**, *111*, 11970–11981.
(25) Li, J. R.; Nilsing, M.; Kondov, I.; Wang, H. B.; Persson, P.; Lunell, S.; Thoss, M. *J. Phys. Chem. C* **2008**, *112*, 12326–12333.
(26) Stier, W.; Prezhdo, O. V. *J. Chem. Phys. B* **2002**, *106*, 8047–8054.
(27) Duncan, W. R.; Stier, W. M.; Prezhdo, O. V. *J. Am. Chem. Soc.* **2005**, *127*, 7941–7951.
(28) Duncan, W. R.; Prezhdo, O. V. *J. Am. Chem. Soc.* **2008**, *130*, 9756–9762.
(29) Fischer, S. A.; Duncan, W. R.; Prezhdo, O. V. *J. Am. Chem. Soc.* **2009**, *131*, 15483–15491.
(30) Rego, L. G. C.; Batista, V. S. *J. Am. Chem. Soc.* **2003**, *125*, 7989–7997.
(31) Abuabara, S. G.; Rego, L. G. C.; Batista, V. S. *J. Am. Chem. Soc.* **2005**, *127*, 18234–18242.
(32) Wang, L.; Willig, F.; May, V. *Mol. Sym.* **2006**, *32*, 765–781.
(33) Jones, D. R.; Troisi, A. *Phys. Chem. Chem. Phys.* **2010**, *12*, 4625–4634.
(34) Martsinovich, N.; Troisi, A. *J. Phys. Chem. C* **2011**, *115*, 11781–11792.
(35) Nilsing, M.; Persson, P.; Lunell, S.; Ojamäe, L. *J. Phys. Chem. C* **2007**, *111*, 12116–12123.
(36) Nilsing, M.; Lunell, S.; Persson, P.; Ojamäe, L. *Surf. Sci.* **2005**, *582*, 49–60.
(37) Ernstorfer, R. *Ph.D. Thesis*, Freie Universität, Berlin, 2004; http://www.diss.fu-berlin.de/2004/268/.
(38) Gundlach, L. *Ph.D. Thesis*, Freie Universität, Berlin, 2005; http://www.diss.fu-berlin.de/2005/269/.
(39) Jakubikova, E.; Snoeberger, R. C.; Batista, V. S.; Martin, R. L.; Batista, E. R. *J. Phys. Chem. A* **2009**, *113*, 12532–12540.
(40) Luschtinetz, R.; Frenzel, J.; Milek, T.; Seifert, G. *J. Phys. Chem. C* **2009**, *113*, 5730–5740.
(41) Pang, C. L.; Watkins, M.; Cabailh, G.; Ferrero, S.; Ngo, L. T.; Chen, Q.; Humphrey, D. S.; Shluger, A. L.; Thornton, G. *J. Phys. Chem. C* **2010**, *114*, 16983–16988.
(42) Bates, S. P.; Kresse, G.; Gillan, M. J. *Surf. Sci.* **1998**, *409*, 336–349.
(43) Vittadini, A.; Selloni, A.; Rotzinger, F. P.; Grätzel, M. *J. Phys. Chem. B* **2000**, *104*, 1300–1306.
(44) Ojamäe, L.; Aulin, C.; Pedersen, H.; Käll, P. O. *J. Colloid Interface Sci.* **2006**, *296*, 71–78.
(45) Martsinovich, N.; Jones, D. R.; Troisi, A. *J. Phys. Chem. C* **2010**, *114*, 22659–22670.
(46) Preat, J.; Jacquemin, D.; Wathelet, V.; André, J. -M.; Perpète, E. A. *J. Phys. Chem. A* **2006**, *110*, 8144–8150.
(47) Preat, J. *J. Phys. Chem. C* **2010**, *114*, 16716–16725.
(48) Kurashige, Y.; Nakajima, T.; Kurashige, S.; Hirao, K.; Nishikitani, Y. *J. Phys. Chem. A* **2007**, *111*, 5544–5548.
(49) Dovesi, R.; Saunders, V. R.; Roetti, C.; Orlando, R.; Zicovich-Wilson, C. M.; Pascale, F.; Civalleri, B.; Doll, K.; Harrison, N. M.; Bush, I. J.; D'Arco, P.; Llunell, M. *CRYSTAL09 User's Manual*; University of Torino: Torino, 2009.
(50) Corà, F. *Mol. Phys.* **2005**, *103*, 2483–2496.
(51) Zicovich-Wilson, C. M.; Bert, A.; Roetti, C.; Dovesi, R.; Saunders, V. R. *J. Chem. Phys.* **2002**, *116*, 1120–1127.
(52) http://www.crystal.unito.it/Basis_Sets/Ptable.html (accessed 04/10/2011).
(53) Becke, A. D. *J. Chem. Phys.* **1993**, *98*, 5648–5652.
(54) Di Valentin, C.; Pacchioni, G.; Selloni, A. *Phys. Rev. Lett.* **2006**, *97*, 166803.
(55) Hara, K.; Sato, T.; Katoh, R.; Furube, A.; Ohga, Y.; Shinpo, A.; Suga, S.; Sayama, K.; Sugihara, H.; Arawara, H. *J. Phys. Chem. B* **2003**, *107*, 597–606.
(56) Perdew, J. P.; Burke, K.; Ernzerhof, M. *Phys. Rev. Lett.* **1996**, *77*, 3865–3868.
(57) Soler, J. M.; Artacho, E.; Gale, J. D.; García, A.; Junquera, J.; Ordejón, P.; Sánchez-Portal, D. *J. Phys.: Condens. Matter* **2002**, *14*, 2745–2779.